Analytic model of the cathode region of a short glow discharge in light gases

V. I. Kolobov
St. Petersburg University, St. Petersburg 198904, Russia

L. D. Tsendin
St. Petersburg Technical University, St. Petersburg 195251, Russia
(Received 4 November 1991; revised manuscript received 8 May 1992)

A self-consistent analytic model of the cathode region of a dc glow discharge is suggested. The description is based on the division of the discharge gap into a space-charge sheath and a plasma region and on an approximate kinetic analysis of different groups of electrons. A one-dimensional short discharge is considered for which the positive column is absent and the energy relaxation length λ_ε of slow untrapped electrons exceeds the gap length L. In this case, a point exists in the negative glow (NG) region where the plasma density has a maximum and the electric field changes sign. Three groups of electrons are treated separately. The first of them includes fast electrons with energies exceeding the first excitation potential ε^*. They are emitted by the cathode surface (primaries) or generated in the cathode fall region. These electrons are responsible for ionization and excitation processes and electron-current transport in the sheath and in the immediately adjacent plasma. The field reversal is caused by the nonlocal ionization in the plasma part of the NG, which is determined by the fast electrons. The slow electrons are subdivided into trapped and intermediate ones. The full energy ε (kinetic plus potential) of the trapped electrons is less than the anode potential $e\phi_a$. These electrons determine the plasma density but give no contribution to the electron current. In the Faraday dark space, the electron current is due to diffusion of the intermediate electrons with energies $e\phi_a < \varepsilon < \varepsilon^*$. A continuous-energy-loss model is used for description of the fast electrons. Simple analytic solutions for the electron-distribution function (EDF) and nonlocal ionization in the sheath and plasma are obtained from the constant-retarding-force approximation. The EDF of the intermediate electrons is close to isotropic. Analytic solutions for it are derived. Coulomb collisions lead in most cases to a Maxwell-Boltzmann distribution of the trapped electrons. Their temperature T_e at $\lambda_\varepsilon > L$ does not depend on x. The plasma density profile is obtained from the ambipolar diffusion equation. The kinetic analysis of the trapped electrons is necessary only for the calculation of T_e and ϕ_a values. A criterion for the field reversal is proposed. The results are compared with experimental and simulation results of other authors.

PACS number(s): 52.80.Hc, 52.20.Fs

I. INTRODUCTION

Processes in the cathode region determine the main characteristics of glow discharges. The recent increase of interest in this field has been stimulated by numerous glow-discharge applications to plasma surface processing, lasers, and other devices. Application of new experimental methods, such as laser optogalvanic spectroscopy, laser-induced fluorescence, and absorption [1–4] have raised significantly the accuracy and volume of information obtained. Detailed numerical simulations [5–8] have proved to be very useful in understanding the main physical mechanisms that are responsible for plasma and electric-field-profile formation. Nevertheless, the development of a self-consistent theory of these phenomena turned out to be a very difficult problem.

A significant difficulty in the analysis is connected with the enormous difference in characteristic energy, space, and density scales. A sheath region with low charged-particle density and large electric field is immediately adjacent to the plasma, where the density exceeds that in the sheath by many orders of magnitude, and the field is very weak and even changes its sign. The electron-distribution function (EDF) in the plasma contains electrons with high energies, $\sim 10-10^3$ eV, which are accelerated in the sheath and are responsible for the excitation and ionization processes. The range of these electrons is considerable. Thus the ionization produced by them is nonlocal. It is determined by the electron-energy spectrum and not by the local electric-field value. Many important phenomena—for example, the physical mechanism of the Faraday dark-space formation—cannot be understood even qualitatively within the framework of a traditional local approach. Consequently, a kinetic description of the fast electrons is in general use now.

On the other hand, diffusion and recombination processes in the low-field plasma region are determined by a large amount of slow electrons with energies $\sim 10^{-2}-10$ eV. For calculation of the plasma density profile, both electron groups are equally important. However, a unified analytical or numerical kinetic treatment of such multiscale distributions and profiles is very labor consuming. It is useful to introduce sharp boundaries between different space and energy regions, where different processes are predominant, to obtain relatively simple solutions in all the regions and then to assemble them in a

 ©1992 The American Physical Society

manner that resembles a jigsaw puzzle. The advantage of such an approach is the physical transparency of analytic results [9]. Besides, scaling laws and similarity rules can be easily derived. The main shortcomings are the relatively low accuracy and the necessity to correctly guess the boundary positions. For example, the conventionally used division of the cathode region into the dark space, the negative glow (NG), and the Faraday dark space (FDS) is based on visual observations. From the physical standpoint, it is far more convenient to single out the ion space-charge sheath, where the electron density is negligible and the field is strong. It consists of the dark space and a part of the NG. The plasma region includes the low-field NG part, the FDS, and its transition into the positive column (PC). Instead of the Poisson equation, the quasineutrality condition can be used in this region. It is preferable to subdivide the plasma into regions with direct and reversed fields, so that ions generated in them are moving to the cathode or to the anode.

In the absence of electron-electron collisions, the energy relaxation length λ_ε of slow electrons is considerable. The electron motion in the low-pressure discharge demands a kinetic description, and in principle cannot be reduced to the conventional hydrodynamic equations. The motion of electrons that belong to different parts of the EDF is almost independent. Thus it is convenient to divide electrons into several groups.

After the papers of Emeleus and co-workers [10,11], experimenters have usually divided the electrons into three distinct groups: primary, secondary, and ultimate. In earlier papers [12–14], it was considered that each group had a Maxwellian distribution with different mean energies. However, there were no physical reasons for such a distribution. Since then, it has been experimentally observed that the energy distributions of primary and secondary electrons may deviate considerably from the Maxwellian ones [15–17].

In the theoretical treatment, electrons were usually subdivided into two groups: bulk and beam [3,5–9]. The threshold between them was selected in such a way that only the fast electrons were responsible for inelastic processes. For a description of the energetic beam electrons, some sort of kinetic theory was used: either Boltzmann [18–22,25], or Monte Carlo [2,5,6,7,18,23–25]. The slow bulk electrons were usually described by fluid models [5–9,22]. Such an approach, however, cannot explain the existence of the two slow electron groups. An unsuccessful attempt to explain such a behavior in the framework of a kinetic approach to slow electrons has been undertaken in Ref. [26]. A correct explanation was suggested in Ref. [5]. If there is a field reversal in the cathode region and electron-electron collisions are rare, then the slow electrons can be divided into two almost independent groups: trapped and free.

Thus we shall divide electrons into three groups. The first of them includes the fast electrons, which possess kinetic energies that far exceed the first excitation potential ε^*. Some of these electrons are generated at the cathode surface, and the rest of them in the high-field sheath region. They are responsible for the ionization and excitation processes, and for the electron current in the sheath and the adjacent plasma region. The electron density in the plasma is mainly due to the trapped electrons, which give no contribution to the current. The electron current in a part of the NG and in the FDS is determined by the untrapped intermediate electrons, with energies less than ε^*. Their energy relaxation length λ_ε, in our case, exceeds the discharge gap L, so they can freely reach the anode. Such a division can be easily performed in atomic gases. We restrict ourselves to this case.

Since the rigorous solution of this complicated self-consistent problem is very cumbersome, we shall describe here a relatively simple analytical approach to the problem. It is based on a strict division of the discharge gap into the two regions—sheath and plasma—and on a separate approximate kinetic analysis of the fast, intermediate, and trapped electrons.

The description of the fast electrons is based on the continuous-energy-loss model. The scattering was neglected. The comparison of this model to numerical simulations for light gases (H_2,He) shows that such a crude approximation does not lead to significant error. The intermediate electrons can be described by the kinetic equation in the two-term approximation. Their EDF is close to isotropic, and decreases almost linearly from the NG to the anode. The density of trapped electrons is considerable, and the Coulomb collisions, in most cases, lead to a Maxwell-Boltzmann distribution. The temperature of the trapped electrons is very low and spatially uniform, since their energy relaxation length λ_ε exceeds the discharge gap L.

The problem of the electric-field reversal has been discussed in numerous publications [2,3,6,27,28]. Precise and reliable measurements of the reversal position in the low-pressure short discharge were performed in Ref. [3]. The local approximation for ionization, i.e., an assumption that the ionization rate is determined by the local electric field, leads to monotonic profiles of the plasma density and potential, even if the diffusion is taken into account [29–31]. In normal and anomalous discharges, the nonlocality of the ionization is considerable. Owing to the nonlocal ionization, many charged particles are generated in the low-field region, where the plasma density peak is formed. If the density gradient is not too small, the field reversal is necessary to retard the electron diffusion. A field configuration that traps the slow electrons is formed, while the ion motion is described by the ambipolar diffusion. In sufficiently long discharges, a second field reversal has to occur near the FDS-PC boundary. The potential and plasma density profiles, the ionization mechanism in the FDS-PC transition, the striation formation in this region, the field reversal criterion, and other important topics cannot be properly understood without the kinetic analysis of the slow electrons.

We shall restrict ourselves mainly to the case of low-pressure short discharge, where only one field reversal occurs. The FDS-PC transition and the high-pressure case with the monotonic potential profile will be treated in detail elsewhere.

In Sec. II of the paper, a simple analysis of fast electrons is given, and expressions for the ionization rate in the sheath and plasma are derived. In Sec. III, the EDF

for the intermediate and trapped electrons is calculated and compared with the experiment. Section IV is devoted to a self-consistent calculation of the electric field in the sheath and plasma region. In Sec. V, the problem of field reversal is discussed and rough criteria are derived.

II. DESCRIPTION OF THE FAST ELECTRONS

The most detailed description of the fast-electron behavior is given by the Monte Carlo simulations [2,5–7,18,23–25]. This procedure is, however, very labor consuming. On the other hand, owing to a lack of cross-section data, a high accuracy cannot be achieved, even in such detailed calculations.

Two main approximations have been used for the fast-electron description. In the single-beam model [3,6,7,32,33], the electrons were assumed to be directed forward and to form a monoenergetic beam. The density and the mean energy values were described by continuity and energy equations. Since the EDF form is rather complicated, this approach seems to be oversimplified.

Far more realistic is the multibeam approach [6,19,32]. Its feasibility critically depends on a reasonable choice of the beam number K. If $K=1$, it reduces to the single-beam case. On the other hand, at $K\rightarrow\infty$, it is equivalent to the direct solution of the Boltzmann equation without scattering [6,20], and demands considerable computational work.

The nonlocal ionization rate is determined by integrating over the fast-electron spectrum. It is relatively insensitive to the EDF details, and we hope that, for a qualitative description, a rather crude model is sufficient. In this section we present such a model, which, to our mind, accounts for the fast-electron statistics in the simplest manner, and gives a physically transparent analytic solution. The scattering influence is small in the light gases (e.g., in H_2, He). We shall restrict ourselves to this case.

A. Continuous-energy-loss model

The characteristic energies of the fast electron are of the order of the cathode potential fall, $e\phi_c\sim 10^2-10^3$ eV. They greatly exceed the excitation ε^* and ionization ε_i energies. Thus it is possible to use the assumption of continuous energy losses [34–38]

$$\frac{dw}{d\xi}=-N\mathfrak{L}(w)-eE(x)\ , \tag{1}$$

where w is the electron kinetic energy, N the neutral particle density, $\mathfrak{L}(w)$ the energy-loss function, ξ the fast-electron path along its trajectory, and x the spatial coordinate. If the scattering is negligible, then $x=\xi$ and the kinetic equation for the fast-electron EDF $F(v,x)$ is

$$v\frac{\partial F}{\partial x}-\frac{eE(x)}{m}\frac{\partial F}{\partial v}-\frac{\partial}{\partial v}\frac{N\mathfrak{L}(w)}{m}F=J(x,v)\ , \tag{2}$$

where $J(x,v)$ is a source term. In this approach, we neglect the discreteness of energy losses, so it is equivalent to the limit $\varepsilon^*,\varepsilon_i\ll w$ in the multibeam approximation [6]. The expression for $\mathfrak{L}(w)$ at high electron energies (the so-called Bethe-Bloch law) is of the form [34,35]

$$\mathfrak{L}(w)=\frac{2\pi Ze^4}{w}\ln\left[\frac{2w}{\varepsilon_i}\right], \tag{3}$$

where ε_i is the mean ionization energy, and Z is the atomic number. For lower energies, $\mathfrak{L}(w)$ has been calculated in numerous publications [39–42]. In Fig. 1, values of $\mathfrak{L}(w)$ are presented for molecular hydrogen and helium. One can see that, at energies up to $\sim 10^3$ eV, expression (3) is not valid, and the $\mathfrak{L}(w)$ variation in the energy interval from several tens to approximately 10^3 eV (most important for the normal discharge and for a slightly anomalous one) is insignificant. So we assume a simple approximation $\mathfrak{L}(w)=\mathfrak{L}_0=$const. Integration of the kinetic equation (2) results in

$$F(v,x)=F_0(v,x)+\int_{x_0(\varepsilon)}^{x}J(x',\varepsilon)\frac{dx'}{v(\varepsilon,x')}\ , \tag{4}$$

where $v(\varepsilon,x)=[2(\varepsilon+e\tilde{\phi}(x))/m]^{1/2}$. Integration is to be performed at the constant "energy" $\varepsilon=w+N\mathfrak{L}_0x-e\phi(x)=w-e\tilde{\phi}(x)$, where $\phi(x)$ is the electrostatic potential, and $x_0(\varepsilon)$ is the left turning point for the electrons with total energy ε [Fig. 2; at $x=x_0(\varepsilon)$, we have $w=0$ and $e\tilde{\phi}(x_0(\varepsilon))=-\varepsilon$]. The first term on the right-hand side of Eq. (4) corresponds to the primary electrons that are emitted by the cathode, the second to the successive generations of secondary electrons in the sheath. Since the force $N\mathfrak{L}_0$ is nonconservative, the fast electrons

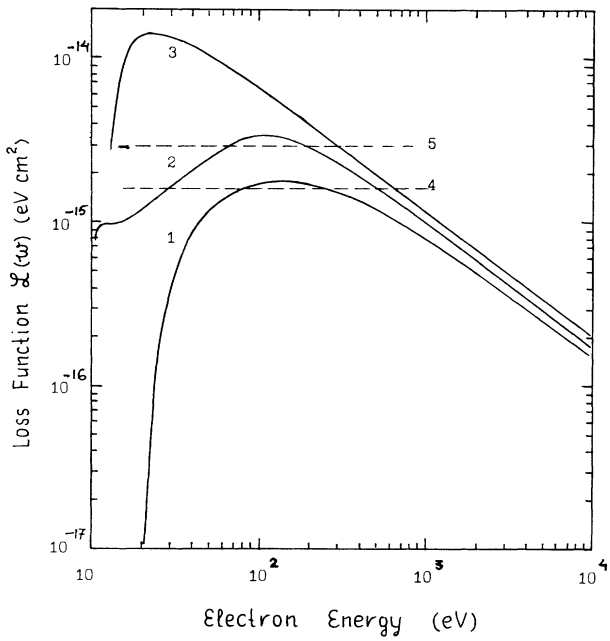

FIG. 1. Energy-loss function $\mathfrak{L}(w)$ for the fast electrons in molecular hydrogen and helium: curve 1 is a calculation [39] for He; curve 2 is a calculation [40] for H_2; curve 3 is a Bethe-Bloch law (3) for H_2; curve 4 is an approximation $\mathfrak{L}(w)=\mathfrak{L}_0=1.5\times10^{-15}$ eV cm^2 for He; curve 5 is an approximation $\mathfrak{L}(w)=\mathfrak{L}_0=3\times10^{-15}$ eV cm^2 for H_2.

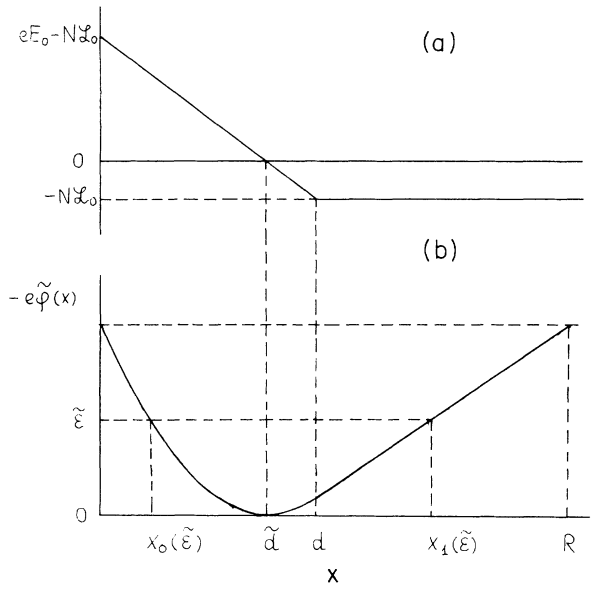

FIG. 2. (a) Total force acting on an electron: $(-eE(x)-N\mathfrak{L}_0)$; (b) effective potential energy of electrons, $e\tilde{\phi}(x)$. Here d is the thickness of the space-charge sheath, $\tilde{d}$ is the point where the total force is zero, and R is the electron range from Eq. (12) for electrons, starting from the cathode surface. The picture is plotted for the linear-field profile in the sheath, when $x_0(\tilde{\varepsilon})=\tilde{d}(1-\sqrt{\tilde{\varepsilon}})$, $x_1(\tilde{\varepsilon})=R-\tilde{\phi}_c R(1-\tilde{\varepsilon})/\phi_c$, $\tilde{d}=d(1-N\mathfrak{L}_0/eE_0)$, $\tilde{\phi}_c=\phi_c(1-N\mathfrak{L}_0/eE_0)^2$. The value of $N\mathfrak{L}_0/eE_0=0.214$ corresponds to a normal discharge in helium with an iron cathode [23].

are stopped at the point $x=x_1(\varepsilon)$ [$x_1(\varepsilon)$ is the right root of the equation $e\tilde{\phi}(x_1(\varepsilon))=-\varepsilon$], and join the intermediate group. Neglecting the starting energy of the primary electrons, we have

$$F_0(v,x)=m\Gamma\delta(\varepsilon-e\tilde{\phi}_c)\ , \tag{5}$$

where Γ is the electron flux from the cathode, $e\tilde{\phi}_c=e\tilde{\phi}(\tilde{d})-N\mathfrak{L}_0\tilde{d}$, and $\tilde{d}$ is the point in the sheath where the total force is equal to zero: $eE(\tilde{d})=N\mathfrak{L}_0$ (see Fig. 2). The secondary electrons are born with small energies, of the order of several eV [39,42]. Neglecting this insignificant energy spreading, and assuming a simple approximation of constant energy loss per ion-electron pair ε_0 [39,43], we have for the source term in Eq. (4)

$$J(v,x)=\delta(v)\int_0^\infty \frac{N\mathfrak{L}_0}{\varepsilon_0}v'dv'F(v',x)$$
$$=v\delta(w)\alpha\int_{-e\tilde{\phi}(x)}^{e\tilde{\phi}_c}F(\varepsilon',x)d\varepsilon'\ , \tag{6}$$

where $\alpha\equiv N\mathfrak{L}_0/\varepsilon_0$. The integral equation for the EDF follows from Eqs. (4)–(6),

$$F(\varepsilon,x)=m\Gamma\delta(\varepsilon-e\tilde{\phi}_c)-\frac{\alpha}{e\tilde{E}(x_0(\varepsilon))}\int_\varepsilon^{e\tilde{\phi}_c}F(\varepsilon',x_0(\varepsilon))d\varepsilon'\ , \tag{7}$$

where $\tilde{E}=-d\tilde{\phi}/dx$. The EDF in Eq. (7) depends only on ε. Multiplying Eq. (7) by $e\tilde{E}(x_0(\varepsilon))$ and differentiating it, we obtain

$$\frac{d}{d\varepsilon}e\tilde{E}(x_0(\varepsilon))F(\varepsilon)$$
$$=\alpha F(\varepsilon)+\frac{d}{d\varepsilon}e\tilde{E}(x_0(\varepsilon))m\Gamma\delta(\varepsilon-e\tilde{\phi}_c)\ . \tag{8}$$

Introducing $\tilde{F}=Fe\tilde{\phi}_c/m\Gamma$ and $\tilde{\varepsilon}=\varepsilon/e\tilde{\phi}_c$, we find the solution of Eq. (8) in the form

$$\tilde{F}(\tilde{\varepsilon})=\delta(\tilde{\varepsilon}-1)-\frac{\alpha\tilde{\phi}_c}{\tilde{E}(x_0(\tilde{\varepsilon}))}\exp(\alpha x_0(\tilde{\varepsilon}))\ . \tag{9}$$

The fast-electron current is

$$j_f(x)=e\int_0^\infty v\,dv\,F(v,x)dv$$
$$=\begin{cases}e\Gamma\exp(\alpha x), & 0<x<\tilde{d},\\ j_f(x_0(\varepsilon=e\tilde{\phi}(x))), & \tilde{d}<x<x_1(e\tilde{\phi}_c)\ .\end{cases} \tag{10}$$

At $x<\tilde{d}$, the total electron current j_e coincides with j_f. Accordingly, in the cathode dark space and in the NG

$$\frac{dj_e}{dx}=\alpha j_f=I(x)\ . \tag{11}$$

The expressions (10) and (11) correspond to a generalization of the conventional Townsend approach with the ionization coefficient $\alpha=$const. In this respect, our model coincides with the model used in Ref. [9]. The only difference is that the ionization density $I(x)$ is proportional now to the fast-electron current j_f instead of the total electron current. The total ionization in the plasma is equal to the fast-electron energy flux from the sheath divided by ε_0 [9].

It is necessary to stress that this result critically depends on the assumption about the energy independence of $\mathfrak{L}(w)$ and $\varepsilon_0(w)$. Generally, the ionization rate depends on the electron-energy spectrum. The latter is formed by the whole potential profile in the sheath, and by the electron-source distribution. Thus, the attempts to introduce, without taking the EDF form into account, some form of the Townsend α, depending, instead of on the local E value, on other local parameters, or on some nonlocal characteristics of the potential profile [44,45], cannot lead, to our mind, to significant progress.

It has been proposed to describe the ionization nonlocality by means of the ionization rate $I(x)$ dependence on the local electron temperature T_e (mean energy) [46–48]. In the sheath, this approach gives reasonable results, because $\mathfrak{L}(w)$ and $\varepsilon_0(w)$ are almost constant here, the slow electrons are absent, and the ionization rate is insensitive to the EDF form. But it is inadequate in the plasma, where the nonlocal ionization is produced by the energetic electrons, and the density and T_e are determined by the slow trapped electrons. As a result, the extraneous peculiarities of the ionization rate arise in this approximation [47,48].

In several publications (see, for example, Refs. [18] and [23]), the approximation $\alpha(\bar{w}(x))$ is used, where $\bar{w}(x)$ is the mean fast-electron energy at x. Since the fast-

electron-energy spectrum is wide and varies considerably with x, such an approximation is based on a rather poor physical foundation. But due to the fact that $\mathfrak{L}(w)$ and ε_0 are nearly constant, the numerical results for the ionization density in the sheath given by this approach are not too bad (curve 3 in Fig. 5). The expression $\alpha(\bar{E}(x))$, where $\bar{E}(x)$ is a certain effective field, was proposed in Refs. [18], [49], and [50]. It also gives reasonable ionization rates in the sheath, but may lead to a significant error in the plasma.

At $x > x_1(e\tilde{\phi}_c)$ from Eqs. (10) and (11), it follows that $I(x)=0$, i.e., the fast electrons do not reach this region. This point can be identified with the boundary between the NG and the FDS. The value of $x_1(e\tilde{\phi}_c)$ can be calculated from Eq. (1) as the range R of the fast electrons with the initial energy $e\phi_c$ [51,52],

$$R(e\phi_c)=x_1(e\tilde{\phi}_c)=\int_0^{e\phi_c}\frac{dw}{N\mathfrak{L}(w)} . \tag{12}$$

In Fig. 3, the NG length values calculated from Eq. (12) and observed in Ref. [51] are compared to the fast-electron range [53].

The parameter $\alpha\tilde{d}$ represents the mean number of avalanches initiated by the fast electrons in the sheath. If the electron-flux multiplication in the sheath is large, then it follows from Eqs. (10) and (11) that the significant decrease of $I(x)$ in the plasma occurs at shorter-than-R distances from the cathode,

$$x-\tilde{d}\sim 1/\alpha \ll R=\frac{e\phi_c}{\alpha\varepsilon_0} . \tag{13}$$

The field in the sheath decreases from its maximum at $x=0$ to approximately zero at $x>d$—the sheath length. For the well-known linear approximation [54]

$$E(x)=\begin{cases}-E_0(1-x/d), & x<d\\ 0, & x>d\end{cases} \tag{14}$$

we have

$$-\tilde{\phi}(x)=\begin{cases}\tilde{\phi}_c(1-x/\tilde{d})^2, & x<d\\ \tilde{\phi}_c+\phi_c(x/R-1), & d<x<R\end{cases}$$

$$\tilde{F}(\tilde{\varepsilon})=\delta(\tilde{\varepsilon}-1)+\frac{\alpha\tilde{d}}{2\sqrt{\tilde{\varepsilon}}}\exp[\alpha\tilde{d}(1-\sqrt{\tilde{\varepsilon}})] . \tag{15}$$

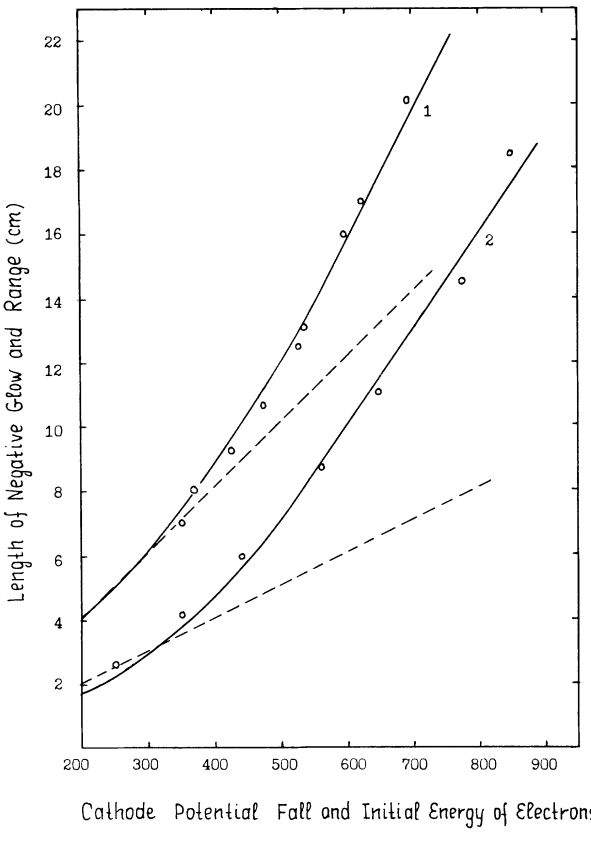

FIG. 3. Comparison of the observed NG length (points [51]) with the fast-electron range (solid line [53]) and with the calculations according to Eq. (12), with $\mathfrak{L}(w)=\mathfrak{L}_0$ (dashed lines). Curve 1 corresponds to helium, curve 2 to hydrogen. Values of $\mathfrak{L}_0$ were chosen according to Fig. 1.

B. The model validity

The proposed model is based on several crude simplifications. Among them, the most obvious ones are the neglect of scattering and of discrete character of the energy losses, as well as the approximation of the constant loss function $\mathfrak{L}(w)$. Therefore we cannot expect to get a precise quantitative description of the experiment. But it is the simplest approach, which accounts for the ionization nonlocality that determines the main characteristics of the NG and the FDS [55].

The error caused by the continuous-energy-loss model is maximum at low energies, i.e., immediately at the cathode surface and at the NG-FDS boundary. The electrons that have not suffered any collisions cannot also be described by this model. The magnitude of these errors can be demonstrated by a comparison to Monte Carlo simulations of Tran, Marode, and Johnson [23], where the EDF and the ionization density in the sheath, with a linearly decreasing electric field, have been calculated for He, without accounting for scattering. In Fig. 4, the EDF of Eq. (15) and the results of Ref. [23] are presented for $\phi_c=150$ eV, $d=1.3$ cm. The small electron-flux multiplication in the sheath (~ 2.5 for these conditions) implies that the primary electron flux [represented by the δ function in Eq. (15)] is considerable throughout the sheath. Energy-loss discreteness leads to spreading of this primary peak, which is roughly proportional to $\sqrt{N\mathfrak{L}_0\varepsilon_i x}$. The Gaussian EDF of the primary electrons with such spreading is shown also in Fig. 4. The value of $\mathfrak{L}_0=1.5\times 10^{-15}$ eV cm^2, accepted in all our calculations, is overstated in this case (see Fig. 1). Nevertheless, one can see that, even in this case, the EDF of Eq. (15) in the medium energy region, which is responsible for the main part of the ionization rate, is not too far from the results of Monte Carlo calculations. The accuracy of the proposed model increases with the increase of electron multi-

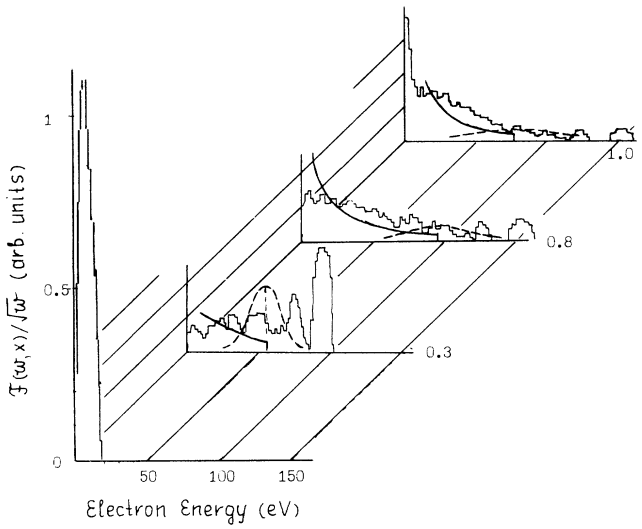

FIG. 4. Electron-energy distribution at various positions in the cathode sheath. Comparison of Monte Carlo simulations [23] (histograms) with calculations according to Eq. (15). Dashed lines correspond to the primary-electron flux.

plication in the sheath (at lower values of γ).

In Fig. 5, values of the effective Townsend coefficient

$$\tilde{\alpha}=\frac{I(x)}{\Gamma+\int_0^x I(x')dx'} \tag{16}$$

are shown according to Eqs. (11) and (14) and to Ref.

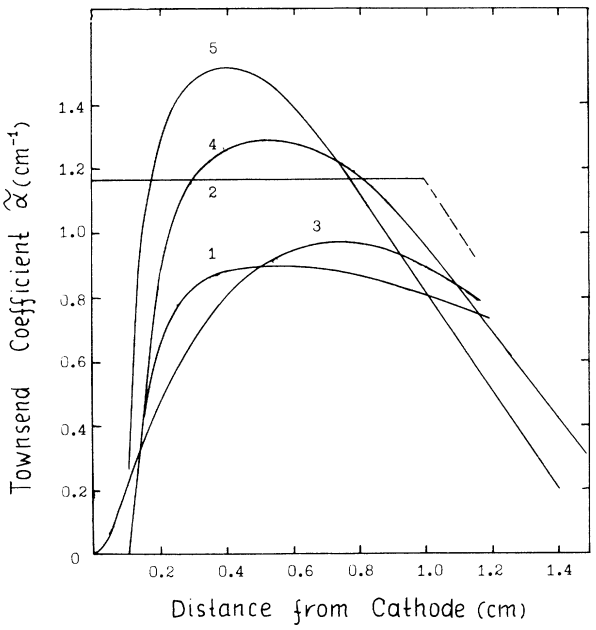

FIG. 5. Effective Townsend coefficient $\tilde{\alpha}$ in the sheath as a function of distance from the cathode: curve 1 is a Monte Carlo simulation [23]; curve 2 is an approximation $\mathfrak{L}(w)=$const, $\varepsilon_0=$const$=46$ eV; curve 3 is an approximation $\alpha(\bar{w})$ [23]; curve 4 is a Monte Carlo simulation [24]; curve 5 is a Monte Carlo simulation [25].

[23]. The zero $\tilde{\alpha}$ values at small x in Ref. [23] correspond to the ionization extinction at $w<\varepsilon_0$, where the continuous-loss model is invalid. The plateau in $\tilde{\alpha}(x)$ dependence in Ref. [23] at the intermediate x values corresponds, to our mind, to the energy independence of ε_0 and $\mathfrak{L}(w)$. The choice of the lower $\mathfrak{L}_0$ value leads to a better agreement with Ref. [23], but we prefer our choice, as it accounts for the scattering to some extent.

C. The scattering influence

This problem is far more complicated. It is well known that, at energies not too large compared to ε^*, the elastic scattering is not far from isotropic, and significantly exceeds the inelastic one [55]. Consequently, the EDF is close to isotropic here. On the other hand, at energies considerably higher than the energies of atomic electrons, all the collisions are Coulomb-like and highly anisotropic [34,35]. The small-angle scattering dominates in this case. At such energies, the loss function is given by Eq. (3). Owing to the scattering, the real electron path along its trajectory x exceeds the distance between the generation and observation points x. This problem has been discussed in Refs. [35] and [56]. If the influence of scattering is small, it can be estimated according to Ref. [35]:

$$\xi=x+\tfrac{2}{3}R\kappa(1-\sqrt{1-x/R}\,)^2\,, \tag{17}$$

where $R(w)$ is the electron range given by Eq. (12), and

$$\kappa=\frac{Z+1}{8}\,\frac{(\ln\{30[w(\mathrm{keV})]/Z^{2/3}\}-1)}{\ln(w/\varepsilon_i)}\,.$$

Since the values of the parameter κ for $Z=1,2$ are small compared to unity, the scattering influence on the electron trajectory in hydrogen or helium is not too significant.

In the considered energy range of $10-10^2$ eV, the angular and energy dependence of the complete set of cross sections is not known. Therefore, even the Monte Carlo calculations are not very reliable in this case, and the results of various authors differ considerably. These differences are mainly due to the choice of an angular dependence of elastic and inelastic cross sections. The one-dimensional Monte Carlo method [23] (which completely neglects the electron scattering) has been transformed by Boeuf and Marode [24] to account for different angular dependences of elastic scattering. An attempt to account for ionization-collision anisotropy has also been undertaken. Ohuchi and Kubota [25] and Schweigert and Schweigert [5] used isotropic elastic scattering. Den Hartog, Doughty, and Lawler [2] used anisotropic elastic scattering, isotropic scattering for excitations, and two different angular dependences for ionizing collisions. Isotropic angular distributions for both outgoing electrons leads to an overestimate of the ionization rate in the abnormal cathode fall in He compared to the experimental data [2]. Boeuf's assumption of anisotropic angular distributions for the ionizing collisions leads to a better agreement with the experiment [2]. The

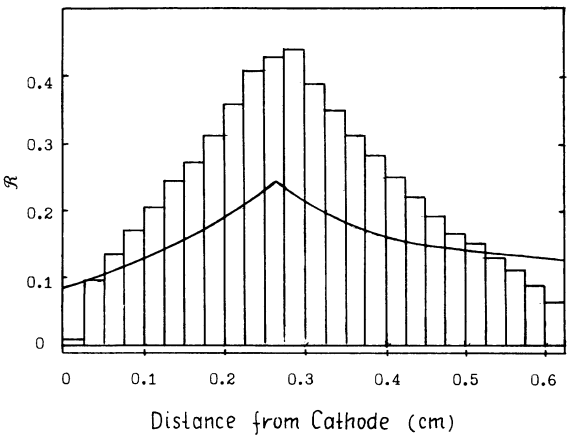

FIG. 6. Ionization rate $\mathcal{R}$ (in units of number of ionizations per electron) as a function of distance from the cathode, for discharge in helium at $p=3.5$ Torr, $j=0.519$ mA/cm^2 [2]. The histogram is a Monte Carlo simulation [2]; the solid line is the calculation according to Eqs. (10), (11), and (14).

fast-electron energy losses for excitation and ionization are comparable: the ε_0 value in Eq. (6) is of the order of $2\varepsilon_i$. Consequently, the isotropic excitation cross sections, used in the kinetic calculations [2], lead to an error of the order of several tens of percent. Such a value is comparable to the error of our simplified model (see Figs. 4–6).

Angular-scattering-probability data in helium, which encompass both elastic and inelastic collisions for energies between 200–1000 eV, demonstrate [57] that the scattering in a forward direction is predominant. This fact also justifies our approach, based on the assumption that, at comparatively low energies, when collisions are not Coulomb-like and Eq. (3) is not applicable, the strong elastic and inelastic scattering anisotropy nevertheless exists, and the electron trajectories in the gases with low Z do not [in accordance with Eq. (17)] differ strongly from the straight lines. The scattering leads to a decrease of the electron penetrating depth and to a growth of the effective $\tilde{\alpha}(x)$ values in the sheath (curves 4, 5 in Fig. 5).

In Fig. 6, the results of the Monte Carlo calculations for the direct ionization spatial distribution in He at $j=0.519$ mA/cm^2, $p=3.5$ Torr, $L=0.62$ cm [2] are compared to calculations according to Eqs. (11) and (12). The discrepancies are mainly caused by the scattering, which leads to a higher ionization at small x and to a steep ionization decrease at large x (compare Fig. 5). It was noted before that the assumption of the isotropic excitation cross section, used in Ref. [2], significantly overestimates, in our opinion, the scattering role.

III. KINETIC EQUATION FOR THE SLOW ELECTRONS

The continuous-energy-loss approximation, described in the preceding section, is valid at $w \gg \varepsilon_i, \varepsilon^*$. Since the characteristic energy of the fast electron is of the order of $e\phi_c$, it is possible to subdivide the fast-electron energies into two intervals, $[e\phi_c, w_0]$ and $[w_0, \varepsilon^*]$, where $e\phi_c \gg w_0 \gg \varepsilon^*$. The continuous-loss approach is applicable to the first of these intervals; the discrete character of the energy loss is essential for the second. The energy dependence of the excitation and ionization cross sections at $w \geq 2\varepsilon^*$ is relatively smooth. The fast electron, during its evolution, quickly passes the energy interval $[w_0, \varepsilon^*]$, and the precise EDF form here is not very important for the calculation of integral characteristics, such as the ionization and excitation rates, which are of primary interest to us.

The situation changes radically at $w < \varepsilon^*$, where the effective energy loss in the excitations and ionizations does not occur. In this energy interval, the elastic and electron-electron collisions are the only energy-relaxation mechanisms and if L exceeds the electron mean transport free path λ, the EDF is close to isotropic and the traditional two-term approximation is valid. It can be used also at the energies slightly exceeding ε^* as soon as $\nu^* \ll \nu$ (ν and ν^* are the transport frequency of elastic and frequency of inelastic collisions, respectively). Introducing the full energy $\varepsilon = w - e\phi(x)$ (note that this definition differs from that used in the preceding section), the kinetic equation for the isotropic part $f_0(\varepsilon, x)$ of the EDF can be written in the form [58–60]

$$\frac{1}{v}\frac{\partial}{\partial x} v D(v) \frac{\partial f_0}{\partial x} + \frac{1}{v}\frac{\partial}{\partial \varepsilon}\left[\delta \nu v w \left[f_0 + T_a \frac{\partial f_0}{\partial \varepsilon}\right]\right] + S_{ee}^{(0)}(f_0) + S^*(f_0) = -\psi(\varepsilon, x) , \tag{18}$$

where δ is the mean energy loss in the collisions with small energy loss (for atomic gases $\delta = 2m/M$; excitation of molecular rotations and vibrations leads to considerably higher δ values in molecular gases), $D = v^2/3\nu$ is the electron diffusion coefficient, T_a is the atomic temperature, $\psi(\varepsilon, x)$ is the source term, $S_{ee}^{(0)}$ is the electron-electron collision integral, and S^* is the inelastic collision integral. If only the first excitation level is important,

$$S^* = \nu^*(\varepsilon, x) f_0(\varepsilon, x) - \left[\frac{w+\varepsilon^*}{w}\right]^{1/2} \nu^*(\varepsilon+\varepsilon^*) f_0(\varepsilon+\varepsilon^*, x) . \tag{19}$$

The expression for $S_{ee}^{(0)}$ is given in Ref. [61]. It can be considerably simplified for collisions of fast electrons, with the slow Maxwellian ones characterized by the density n_s and temperature T_e:

$$S_{ee} = \frac{1}{v}\frac{\partial}{\partial \varepsilon} 2vw\nu_{ee}(w, x)\left[f_0 + T_e \frac{\partial f_0}{\partial \varepsilon}\right] , \tag{20}$$

where $\nu_{ee}(w, x) = \pi n_s(x) e^4 v \Lambda / w^2$, and Λ is the Coulomb logarithm. The numerical calculations (see, for example, Ref. [62]) demonstrate that the approximation (20) does not lead to significant errors. The boundary conditions for Eq. (18) can be taken as

$$\frac{\partial f_0}{\partial x}(x=d)=0, \quad f_0(x=L)=0 \ . \tag{21}$$

In the absorbing-wall approximation $\nu^* \to \infty$, the boundary condition at $\varepsilon+e\phi(x)=\varepsilon^*$ is

$$f_0=0 \ . \tag{22}$$

The slow-electron density is

$$n_s(x)=\frac{4\pi}{m}\int_{-e\phi(x)}^{\varepsilon^*} v(\varepsilon,x)f_0(\varepsilon,x)d\varepsilon \ . \tag{23}$$

The current density transported by these electrons is

$$j_s(x)=\frac{4\pi e}{3m}\int_{-e\phi(x)}^{\varepsilon^*} v(\varepsilon,x)D(\varepsilon,x)\frac{\partial f_0}{\partial x}d\varepsilon \ . \tag{24}$$

Three main processes determine the source term $\psi(\varepsilon,x)$ in Eq. (18). The first of them corresponds to degradation of the fast electrons injected into the plasma from the cathode sheath. In the unit plasma volume $N\mathfrak{L}_0F(w=0,x)/m$, fast electrons are stopped during the unit time [where $F(w,x)$ is given by Eqs. (9) and (15)]. Their energy spectrum is determined by various excitation and ionization processes; the simplest model corresponds to the uniform generation of the slow electrons in the energy interval $w<\varepsilon^*$:

$$\psi_1(\varepsilon,x)=\frac{N\mathfrak{L}_0}{\frac{8\pi}{3}\varepsilon^*(2\varepsilon^*/m)^{1/2}}F(w=0,x) \ . \tag{25}$$

The second source is connected with the slow electrons generated in the plasma by the fast-electron impact:

$$\psi_2(\varepsilon,x)=\frac{N}{v(\varepsilon,x)}\int_0^{\infty}F(w',x)\sigma_{ii}(w',w)dw' \ , \tag{26}$$

where $\sigma_{ii}(w',w)$ is the differential ionization cross section [40].

If the first excited state is metastable (or if the radiation for the transition $1\to0$ is considerably trapped), the superelastic collisions of the slow electrons with the energy gain ε^* lead to generation of electrons with kinetic energy slightly exceeding ε^*. The corresponding source term is [63]

$$\psi_3(\varepsilon,x)=N^*(x)(w-\varepsilon^*)\sigma^*(w-\varepsilon^*)\sqrt{2/mw} \times f_0(w-\varepsilon^*,x) \ , \tag{27}$$

where $N^*(x)$ is the metastable density and σ^* is the superelastic collision cross section. Other plasma-chemical processes, such as chemoionization, also give the corresponding source terms [64].

The electron with the energy $w\sim\varepsilon^*$ reaches the anode during the time $\tau_1\sim(L-d)^2/D$. The simplest case corresponds to relatively low plasma density, when this time is small compared to ν_{ee}^{-1}, see Eq. (20), and to the low-pressure short discharge:

$$L \ll \lambda_\varepsilon=\frac{\lambda}{\sqrt{\delta}} \ , \tag{28a}$$

$$L \ll l_D=\sqrt{D_a\tau} \ . \tag{28b}$$

In this case it is possible to subdivide the slow electrons into two groups. For the intermediate group, with $\varepsilon^*>\varepsilon>e\phi_a$ (ϕ_a is the anode potential) in kinetic equation (18), only the space diffusion and the source terms are to be left. The EDF for this energy region is [65]

$$f_0^{(i)}=\int_x^L\frac{dx'}{v(\varepsilon,x')D(\varepsilon,x')}\int_d^{x'}v(\varepsilon,x'')\psi(\varepsilon,x'')dx'' \ . \tag{29}$$

From Eq. (28a), it follows that the EDF of the trapped electrons $f_0^{(t)}(\varepsilon,x)$ depends on ε only. If, for these electrons, $\nu_{ee}\gg\delta\nu$, and the source term can be neglected, from Eq. (18) the Maxwell-Boltzmann expression follows:

$$f_0^{(t)}(\varepsilon)=\left[\frac{m}{2\pi T_e}\right]^{2/3}n_m[\exp(-\varepsilon/T_e) -\exp(-e\phi_a/T_e)] \ . \tag{30}$$

Here n_m is the maximum trapped electron density at the point of the field reversal $E(x)=0$. The value of T_e in Eq. (30) can be found from the integral energy balance for the trapped electrons:

$$\int_0^{e\phi_a}\frac{d\varepsilon}{m}\int_{x_-(\varepsilon)}^{x_+(\varepsilon)}dx\ w(\varepsilon,x)\frac{\partial}{\partial\varepsilon}\left[\delta\nu v w f_0^{(t)}\left[1-\frac{T_a}{T_e}\right]\right]+W_{it}+W_{ft}=\int_0^{e\phi_a}\frac{d\varepsilon}{m}\int_{x_-(\varepsilon)}^{x_+(\varepsilon)}dx\ wv\psi(\varepsilon,x) \ , \tag{31}$$

where $x_\pm(\varepsilon)$ are the turning points for the electron with total energy ε, defined as the roots of the equation $\varepsilon-e\phi(x_\pm(\varepsilon))=0$. The power transferred to the trapped electrons from the intermediate ones is

$$W_{it}=\int_{e\phi_a}^{\varepsilon^*}\frac{d\varepsilon}{m}\int_{x_-(\varepsilon)}^{L}w(\varepsilon,x)\frac{\partial}{\partial\varepsilon}(2v^3\nu_{ee}f_0^{(e)})dx \sim n^{(i)}\nu_{ee}(\varepsilon^*)\varepsilon^* \ , \tag{32}$$

where

$$n^{(i)}(x)=\frac{4\pi}{m}\int_{e\phi_a}^{\varepsilon^*}v(\varepsilon,x)f_0(\varepsilon,x)d\varepsilon \tag{33}$$

is the intermediate electron density; the expression for the power transferred from the fast electrons W_{ft} is similar.

The problem of the energy balance for the trapped electrons, Eq. (31), is rather complicated. The value of T_e is sensitive to the EDF form in the vicinity of $\varepsilon=e\phi_a$, where neither Eq. (29) nor Eq. (30) is valid. A significant simplification is possible if the source term in Eq. (31) can be neglected. For the ψ_1 source, Eq. (25), for example, the slow-electron generation rate is of the order of $(e\phi_a/\varepsilon^*)^{3/2}n^{(i)}/\tau_1$. From $e\phi_a\sim T_e$, it follows that the contribution of this source term to Eq. (31) can be neglected, if

$$\tau_1 \nu_{ee}(\varepsilon^*) > (T_e/\varepsilon^*)^{5/2} .$$

A systematic experimental investigation of the slow-electron EDF in such short discharges has not been performed. In Ref. [4], the slow-electron temperature and n_m were measured in He at $p=3.5$ Torr, $L=0.62$ cm, $j=0.8$ mA/cm^2. Calculations according to Eqs. (31) and (32), with the EDF of the intermediate electrons given by formula (29) and the EDF of the fast electrons given by Eq. (15), with the experimental field profile in the sheath (which is close to the self-consistent one—see Sec. IV), results in the trapped-electron temperature value $T_e=0.1$ eV, which is close to the experimental value 0.12 eV.

Relaxation of the EDF in He at $p=4$ Torr in the intermediate-energy region was observed in Ref. [17]. The electrode gap $L=2$ cm exceeded $\lambda_\varepsilon=1.7$ cm, and was small compared to the length $[D/\nu_{ee}(\varepsilon^*)]^{1/2}=6$ cm at $n_s=10^{11}$ cm^{-3}, which corresponds to formation of the Maxwellian EDF for the intermediate electrons. The influence of the small plasma field on the intermediate electrons can be neglected ($\varepsilon^* \gg T_e$). In this case, the kinetic equation (18) can be reduced to the diffusion one

$$\frac{\partial \Phi}{\partial t} = \frac{\partial^2 \Phi}{\partial x^2} + \Psi(x,t) , \tag{34}$$

where the variables $\Phi(x,t)=\delta v v w f_0^{(t)}(x,w)$ and $t = \int_w^{\varepsilon^*} 2dw'/3\delta\nu^2 mv$ are introduced [66], and the source $\Psi(x,t)$ is $\Psi=3\delta\nu^2 mv\psi/2$. The boundary conditions (21) and (22) are of the form

$$\frac{\partial \Phi}{\partial x}(x=d)=0, \quad \Phi(x,t=0)=0, \quad \Phi \to 0 \text{ at } x \to \infty . \tag{35}$$

The solution of the diffusion problem (34) and (35) can be written as

$$\Phi(x,t)=\frac{1}{2\sqrt{\pi}} \int_0^t dt' \int_{-\infty}^{\infty} dx' \frac{\Psi(d+|x'|,t')}{\sqrt{t-t'}} \times \exp\left[-\frac{(x-d-x')^2}{4(t-t')}\right] . \tag{36}$$

The different electron sources give additive contributions to the function $\Phi(x,t)$. The sources ψ_1 and ψ_2, see Eqs. (25) and (26), depend weakly on energy. On the contrary, the source ψ_3, Eq. (27), of electrons that have been generated in the superelastic collisions of slow electrons with metastables or in metastable collisions with each other, can be approximated by the δ function of energy. In Fig. 7, a comparison of the EDF calculated from Eq. (36) and that observed in Ref. [17] is shown. Two source terms ψ_3, with initial energies 15.0 eV and 19.8 eV, existed in the plasma, corresponding to the intermediate-electron generation in the collisions between metastable atoms and in the collisions of slow electrons with the metastables. The dashed lines in Fig. 7 represent the EDF of Eq. (36) at the points $x-d=0$, 4, 8 mm. A spatial dependence of the second source term was chosen in the simplest form of $\Theta(x_m-x)$, where Θ is the step function and x_m is given by Eq. (42). The qualitative agreement between the calculated and observed EDF is clearly seen. The differences can be attributed (a) to a model spatial dependence of the source term; (b) to a contribution of the remaining source terms; and (c) to whether the x values in the experiment correspond to the distance from the cathode surface or from the sheath boundary.

The electron current in the sheath coincides with the fast-electron current j_f. In the plasma at $d<x<R$, the transformation from j_f to j_s, see Eqs. (10) and (24), occurs, and at $R<x<L$ (in the FDS), the electron current coincides with j_s. The trapped electrons, as a rule, give the main contribution to the plasma density, Eq. (23), but zero contribution to the current j_s.

The total electron current j_s in the FDS is transported by diffusion of the untrapped intermediate electrons. It can be roughly approximated as $j_s \sim D^{(i)} dn^{(i)}/dx$, where $D^{(i)} \sim D(\varepsilon^*)$ is the mean intermediate-electron diffusion coefficient, Eq. (18), and the density $n^{(i)}$ is given by Eq. (33). The density of the trapped electrons exceeds $n^{(i)}$ by orders of magnitude, but their current is exactly equal to zero. The traditional approach employs the division of the slow-electron current into diffusion and drift ones:

$$\frac{j_s}{e} = D^{(s)} \frac{dn_s}{dx} - \mu_e n_s E . \tag{37}$$

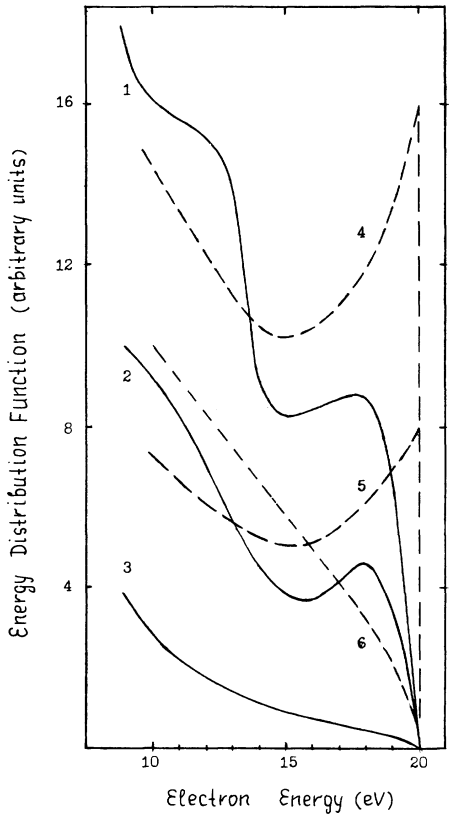

FIG. 7. Energy distribution of intermediate electrons at various positions within the plasma. Comparison of the experimental data [17] (solid lines at x: 1–2 mm; 2–8 mm; 3–14 mm) with calculation according to Eq. (36) [dashed lines at $(x-d)$: 4–0; 5–4 mm, 6–8 mm].

But the trapped and untrapped electron densities $n^{(t)}(x)$ and $n^{(i)}(x)$ vary along the FDS in an entirely different manner. Since the electron current is transported only by the untrapped electrons, it is in principle impossible to express j_s in terms of total n_s density (and its derivatives). Therefore, Eq. (37) is altogether misleading in this case, and can result in substantial errors. Attempts to express the current j_s in terms of other characteristics averaged over the entire EDF (e.g., electron temperature), or an addition of the thermodiffusion term [22,47,67] to Eq. (37), do not substantially improve its accuracy. From the physical point of view, the effective electron temperature variation along the FDS [67] is due to a variation of the ratio between the trapped-electron density (with uniform temperature) and the density of the intermediate ones (with the energy of the order of ε^*).

IV. THE PLASMA-DENSITY PROFILE AND THE SHEATH STRUCTURE

The quasineutral region is traditionally described by the ambipolar diffusion equation [5,9]. For a current-carrying inhomogeneous plasma, such an approach is valid only in the case of a simple isothermal plasma that consists of electrons and one species of positive ion with field- and density-independent mobilities. The violation of these assumptions results in considerable complications. If the mobilities are field-dependent, or more than one ion species is present, the ambipolar drift phenomenon is significant [68,69]. Since ambipolar drift velocity is usually anode directed and of the order of ion drift velocity, this effect leads to the FDS spatial scale $\sim\mu_i E\tau$ instead of the above-mentioned scale l_D, Eq. (28b).

In the low-pressure case, when the inequality (28a) holds, the trapped electrons are isothermal, and the ion profile is determined with high accuracy by the ambipolar diffusion equation, with the source term defined by Eq. (11):

$$\frac{d}{dx}D_a\frac{dn}{dx}+I(x)-\frac{n}{\tau}=0 \ . \tag{38}$$

Zero conditions at the boundaries between the plasma and the anode and cathode sheaths are a good approximation [9]. The more precise boundary conditions are obtained below [Eqs. (44) and (45); for a detailed discussion, see Ref. [70]].

The electron density in the plasma is determined mainly by the trapped electrons with the Maxwell-Boltzmann EDF (30). Accordingly, the electrostatic potential is given by $e\phi(x)=-T_e\ln(n/n_m)$, where the density maximum at $x=x_m$ corresponds to the field-reversal point and the T_e value is determined by Eq. (31). The close correlation between the field-reversal position and the density maximum was observed in experiments [3] and in calculations [3,5–7].

Solution of Eq. (38) with the zero conditions $n(L)=n(d)=0$ is of the form

$$n(x)=\int_d^L G(x,y)I(y)dy \ , \tag{39}$$

where $G(x,y)$ is the Green function. The position of the density maximum $x=x_m$ is determined by the equation

$$\int_d^L \frac{\partial G(x_m,y)}{\partial x}I(y)dy=0 \ . \tag{40}$$

The ions generated at $x>x_m$ are driven to the anode; those generated at $x<x_m$ are returned to the cathode. In the absence of recombination, a considerable amount of the ions returns to the cathode. The recombination is negligible if the plasma length is small compared to the diffusion length, i.e., $(L-d)\ll l_D$. In this case the Green function $G(x,y)$ has the simplest form

$$G(x,y)=\frac{1}{D_a(L-d)^2}\times\begin{cases}(x-d)(L-y), & d<x<y\\ (L-x)(y-d), & y<x<L\end{cases} . \tag{41}$$

Using Eq. (41) for the Green function, we obtain from Eq. (40) the equation for x_m:

$$\int_d^L xI(x)dx=(L+d)\int_{x_m}^L I(x)dx \ . \tag{42}$$

If the FDS length $L-R$ exceeds $R-d$, it follows from Eq. (42) that, as $x_m\to R$, the majority of plasma-generated ions return to the cathode. In the case when $R-d$ exceeds $L-R$, the majority of fast electrons reach the anode, and ionization in the plasma part of the NG is almost uniform and, according to Eq. (10), is given by $I(x)\cong I_0=N\mathcal{L}_0 j_f(d)/e\varepsilon_0$. In this case, $x_m=(L+d)/2$. The ion-current values at $x=d$ and L in this case are almost equal, and the plasma-density profile is close to parabolic, with $n_m=I_0(L-d)^2/8D_a$.

In the experiments [2], the values of R exceeded the gap value $L=0.62$ cm (see Table I). This means that approximately half of the ions generated in the plasma return to the cathode. In calculations [2], it was postulated that ions generated in the plasma do not reach the cathode. This corresponds to the identification of the field-reversal point, $x=x_m$, with the sheath boundary, $x=d$. Such an approach underestimates the ion flux to the cathode; thus higher values of ϕ_c are necessary when compared to the ones calculated by taking into account the ion flux from the plasma. The difference can be significant, especially in the highly anomalous discharge case.

The boundary plasma density n_b at $x=d$ may be estimated as follows. Let us determine the sheath boundary as a point, where the deviation from quasineutrality

$$n_i-n_e=\frac{1}{4\pi e}\frac{dE}{dx} \ , \tag{43}$$

which is necessary for formation of the quasineutral field profile with the ambipolar potential $\phi=-(T_e/e)\ln[n(x)]$, is of the order of n_e. The ion flux in the vicinity of the sheath boundary is $\Gamma_i(x)\cong -D_a dn/dx\cong\Gamma_0=\Gamma_i(x=d)\cong -D_a n_m/(x_n-d)$. This flux can be approximately derived from the ambipolar diffusion equation (38), with the zero boundary condition at $x=d$. In this way, we obtain the boundary density

TABLE I. Discharge parameters for short discharges in helium at $p=3.5$ Torr. Comparison of the experimentally observed (upper entries; [2]) and calculated (lower entries) values of the field at the cathode surface E_0 and the sheath thickness d.

Parameters \ j (mA/cm^2)	0.190	0.519	0.846	1.18	1.50
E_0 (kV/cm)	0.897	1.426	1.870	2.395	3.017
	0.96	1.56	2.04	2.54	3.28
d (cm)	0.382	0.301	0.282	0.300	0.396
	0.19	0.21	0.24	0.28	0.40
ϕ_c (V)	171	215	264	359	597
$E_0/j^{2/3}$	2.72	1.77	2.09	2.14	2.30
R (cm)	0.955	1.24	1.60	2.36	4.66

$$n_b=\left[\frac{\Gamma_0 T_e}{4\pi e^2 D_a^2}\right]^{1/3} \tag{44}$$

for the case of field-independent ion mobility in the plasma. If the field at $x>d$ is considerable, i.e., $eE(d)\lambda_i>T_a$, the ambipolar diffusion coefficient is field dependent. For a widely used approximation $\mu_i(E)=k_i/\sqrt{E}$, we have for this case

$$n_b=\left[\frac{\Gamma_0^4}{2\pi k_i^4 T_e}\right]^{1/5} . \tag{45}$$

The transition region between the sheath and the plasma was investigated in more detail in Refs. [5] and [70].

The field profile in the sheath (for $0<x<d$) is determined by the Poisson equation

$$\frac{dE}{dx}=4\pi e\frac{\Gamma_i(x)}{\mu_i(E)E} , \tag{46}$$

where the ion flux $\Gamma_i(x)$ is given by the continuity equation

$$\frac{d\Gamma_i}{dx}=I(x)=\alpha\Gamma_e(x) . \tag{47}$$

The boundary conditions are

$$\gamma\Gamma_i(0)=\Gamma_e(0)=\Gamma, \quad \Gamma_i(d)=\Gamma_0=j_0/e . \tag{48}$$

The ion flux at the sheath edge Γ_0 can be calculated as

$$\Gamma_0=\int_d^{x_m} I(x)dx . \tag{49}$$

Substituting the expression for $I(x)$ from Eq. (10) and integrating Eqs. (46) and (47), with $\mu_i(E)=k_i/\sqrt{E}$, we obtain the field profile in the sheath

$$E^{3/2}(x)=\frac{6\pi j}{k_i}\left[d-x-\frac{\gamma}{\alpha(1+\gamma)}(e^{\alpha d}-e^{\alpha x})\right] . \tag{50}$$

As was mentioned in Sec. II, our simple kinetic model is equivalent, in the main part of the sheath, to the fluid model with $\alpha=$const. Accordingly, the expressions (46)–(50) coincide with the ones derived by Weizel, Rompe, and Schon [9].

The field profile given by Eq. (50) can, in principle, strongly deviate from a linear one (14). In the limiting case $\alpha d\ll 1$, when the ionization in the sheath is negligible, it follows from Eq. (50) that $E/E_0=(1-x/d)^{2/3}$. Such profiles were observed in Ref. [71]. The ion generation in the sheath leads to the decrease of dE/dx values in the vicinity of $x=d$, and to deviation of the $E^{3/2}(x)$ profile (50) from a linear one (Fig. 8). The $\mu_i(E)$ dependence and the ion-flux nonconservation in the sheath result in the opposite deviations from a linear $E(x)$ profile. As a result, nearly linear $E(x)$ profiles are often formed, such as were observed in Ref. [2] (Fig. 8).

The sheath thickness d is determined from Eq. (50) as a point, where $E(d)=0$:

$$d=\frac{1}{\alpha}\ln\frac{(j-j_0)(1+\gamma)}{\gamma j} . \tag{51}$$

The expressions (49)–(51) give the E_0 and d values, and

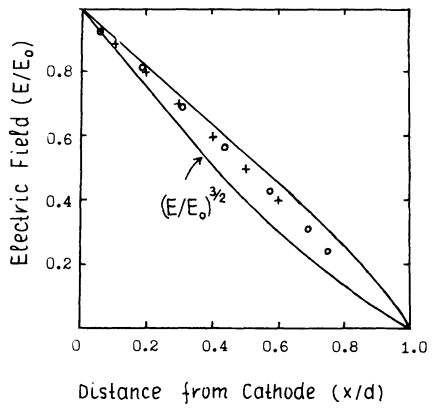

FIG. 8. Electric-field profile vs the distance from the cathode in the sheath for the experimental conditions of Ref. [2]: points are the experimental data [2]; solid line is the calculation according to Eq. (50).

determine their dependence on j, L, γ. In experiment [2], the fast-electron range R significantly exceeded L (see Table I). In this case, the plasma-density profiles should be parabolic, with n_m proportional to the current density. In the approximation $\mathfrak{L}(w)=\text{const}$, $\varepsilon_0=\text{const}$, the sheath thickness should be current independent; the electric field at the cathode surface and discharge voltage should be proportional to $j^{2/3}$. Equation (51) for αd can be reduced for this case to

$$e^{\alpha d}\left[1+\frac{\alpha}{2}(L-d)\right]=1+\frac{1}{\gamma} . \tag{52}$$

The current dependence of the d values calculated according to Eq. (52), which are presented in Table I, is caused mainly by the gas heating. The discrepancy between the calculated and observed d values at low currents is mainly determined by the significant violation of the $\mathfrak{L}(w)=\text{const}$, $\varepsilon_0=\text{const}$ approximation in this case (see Fig. 1). The range values R at low currents were comparable with L, and the inhomogeneity of the ionization rate in the plasma was considerable. These circumstances also result in the lowering of the ion flux from the plasma, and in an additional increase of the (αd) values compared with Eq. (52). The values of the field E_0 in Table I were calculated according to Eq. (50) with the observed d values. It turned out in Ref. [2] that the observed ion-flux values at the cathode surface [which are proportional to $dE/dx\,(x=0)$] were equal to a calculated value of $\int_0^d I(x)dx$. From this fact, it was deduced that the ion flux from the plasma was equal to zero. Accordingly, the field-reversal point was identified with the sheath boundary. In our opinion, this coincidence rather characterizes the reliability of Monte Carlo calculations [2]. The ionization rate $I(x)$ in our calculations was about 30% lower than in Ref. [2] (see Fig. 6). With this reduced value, the flux at the cathode observed in Ref. [2] was equal to the sum of the ionization in the sheath and one-half of the plasma ionization.

V. ELECTRIC-FIELD REVERSAL CRITERIA AND FDS-PC TRANSITION

It is widely known now that nonlocal ionization in the NG plasma is necessary for the existence of the field reversal. But it was not clear whether this was sufficient for realization of such a reversal, or whether some additional criteria were necessary. In Ref. [7], it was pointed out that the field reversal occurred if the slow-electron diffusion current exceeded the total electron current. Since the field-reversal problem is rather complicated and many-parametric, we restrict ourselves to the simple case of a density-independent τ, as in Eq. (38).

A. High pressure

The ambipolar diffusion equation (38), with account taken for thermal diffusion, is applicable also at high pressures, when the FDS length L_F exceeds the length λ_ε, Eq. (28a), if the electron mobility μ_e is a constant (such an approximation is traditionally used for He and H_2) and one ion species is present. In this case, Eq. (37) is valid. Addition of the thermal diffusion term [22,74], which does not exceed the diffusion term in Eq. (37), as a rule, does not change the plasma profile qualitatively. An ionization term I_2, due to the plasma electrons, should be added into Eq. (38). This term depends on the magnitude of the local field, i.e., $I_2=I_2(E)$. The corresponding solution of Eq. (38), in a spatially semi-infinite case, describes the exponential density decrease in the FDS from n_m to $n_c \ll n_m$, with the characteristic scale l_D given by Eq. (28b):

$$n \cong n_m \exp[-(x-x_m)/l_D] . \tag{53}$$

The field and density in the PC are determined by $I_2(E_c)=n_c/\tau_c$. Accordingly, in the long discharge, we have

$$L_F \cong l_D \ln(n_m/n_c) . \tag{54}$$

Near the FDS end, $x=x_m+L_F$, the ionization I_2 steeply increases, the expression (53) is no longer valid, and the transition to the PC occurs.

If, for example, the wall recombination in the FDS dominates, in conventional cylindrical geometry, $l_D=\Lambda/2.4$ (Λ being the chamber radius). In the case where $l=(x_m-d)<l_D$ (see Fig. 9), the ion flux from the plasma into the sheath constitutes, according to Eqs. (49) and (40), a considerable part of the total current. Consequently,

$$D_a(T_e^{(0)})n_m/l \sim j/e=\mu_e n_c E_c , \tag{55}$$

where $T_e^{(0)}$ corresponds to $x=x_m$. Using $D_e=T_e^{(0)}\mu_e/e$, and comparing Eqs. (37) and (55), we obtain

$$E(x)=\frac{T_e^{(0)}\mu_i}{l\mu_e}\left[\exp[-(x-x_m)/l_D]-\frac{l\mu_e}{l_D\mu_i}\right] . \tag{56}$$

Thus, at sufficiently high pressures, when

$$\frac{l_D\mu_i}{l\mu_e}>1 , \tag{57}$$

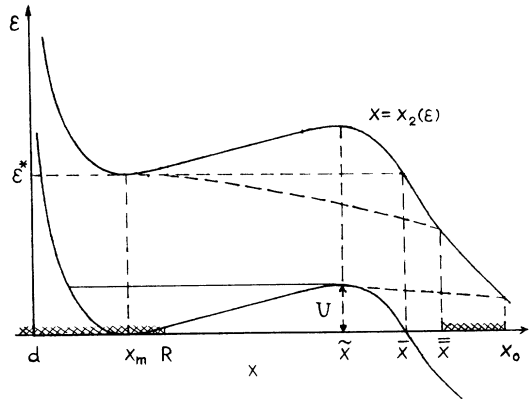

FIG. 9. The potential profile in the NG-FDS-PC region of the long low-pressure discharge. The curve $x=x_2(\varepsilon)$ is defined according to $\varepsilon-\varepsilon^*=e\phi(x_2(\varepsilon))$. The dashed lines show schematically the intermediate-electron energy degradation due to elastic collisions.

the field reversal is absent. The ion flux Γ_i is cathode directed in the whole discharge gap. It is generated at the anode sheath, remains constant ($\Gamma_{ic}=\mu_i n_c E_c$) in the PC, decreases in the FDS, and steeply increases in the NG. The characteristic scale $l\mu_e/\mu_i$ is proportional to the fast-electron range (12), and essentially exceeds the slow-electron energy-relaxation length λ_ε. Consequently, at $l_D > \lambda_\varepsilon$, the slow-electron energy transport is negligible, and the effective temperature T_e of these electrons is determined by a local balance of the Joule heating and energy losses due to collisions. Since the plasma density in the FDS varies exponentially, the field variation according to Eq. (56) is also very considerable. The T_e variation along the FDS can be roughly estimated from Ref. [69] as

$$T_e(x)=T_e^{(0)}+e\langle E\rangle\lambda_\varepsilon , \tag{58}$$

where $\langle E\rangle$ is the heating field (direct field in the FDS) averaged over the length of the order of λ_ε. Since λ_ε in atomic gases exceeds 1, as a rule, the $T_e^{(0)}$ value corresponds to $x=x_m+\lambda_\varepsilon$, and the monotonic growth of $T_e(x)$ with distance follows from Eq. (58).

With the pressure decrease, two field-reversal points appear. One of them is slightly displaced towards the anode with respect to x_m. This displacement can be easily found from Eqs. (37) and (53). The position of the second reversal $\bar{x}$ moves towards the PC boundary as the pressure decreases:

$$\bar{x}-x_m=l_D\ln\left[\frac{n_m T_e^{(c)}}{el_D n_c E_c}\right]<L_F , \tag{59}$$

where $T_e^{(c)}=eD_e(E_c)/\mu_e(E_c)$ is the electron temperature in the PC, the ratio $T_e^{(c)}/eE_c=\lambda_\varepsilon^{(c)}$ being the energy-relaxation length in the PC. The retarding field at $x<x_m$ (and at $\bar{x}>x>x_m$ if the field reversal exists) should not be included into the $\langle E\rangle$ value. Consequently, at $l\mu_e/\mu_i > l_D > \lambda_\varepsilon$, the $T_e(x)$ profile in the reversed-field region is uniform and $T_e\cong T_a$. At $x>\bar{x}$, the electron heating is considerable, and $T_e(x)$ varies up to two orders of magnitude.

If the slow-electron collision frequency is energy dependent, then at some point the dependence $\mu_e(T_e)$ becomes significant, and the density-profile characteristic scale increases from l_D up to the value of the order of $\mu_i E\tau \gg l_D$ [68,69].

In the short high-pressure discharge, when the gap length L is less than the L_F given by Eq. (54), the PC is absent. In the case where Eq. (57) holds, a positive anode fall is expected. If $L<\bar{x}$, the anode fall will be negative.

B. Low pressure

If the energy-relaxation length λ_ε does not vary significantly with the energy, comparing Eq. (54) with Eq. (59), we see that at low pressures, when $\lambda_\varepsilon > l_D$, the reversed-field region occupies practically the entire FDS length. The slow trapped electrons are isothermal, and the ambipolar diffusion equation (38) is applicable in this case, too; the intermediate electrons are to be treated kinetically according to Eqs. (29) and (36).

In the short discharge, $(L-x_m)<l_D$, which has been treated in the preceding sections, the FDS was adjacent to a negative anode potential fall (of the order of T_e/e), and the ions generated at $x>x_m$ moved towards the anode. In the case of the long discharge, the second field reversal occurs at the FDS-PC boundary, and the PC stretches out to a positive anode fall [72]. The FDS and the FDS-PC transition region are sketched in Fig. 9. The potential profile here is determined by the equation

$$\mu_i\frac{d}{dx}nE=I(x)-\frac{n}{\tau} , \tag{60}$$

where a connection between the plasma density and the potential is given by Eqs. (23), (30), and (33):

$$n(x)=n^{(i)}(x)+n_m[\exp(-e\phi/T_e)+\exp(-U)] . \tag{61}$$

The intermediate electron density $n^{(i)}(x)$ is to be calculated according to Eq. (29), where the upper integration limit is to be replaced by $x=x_2(\varepsilon)$, where $e\phi(x_2(\varepsilon))=\varepsilon^*-\varepsilon$. The trapped electron density [the second term in the right-hand side of Eq. (61)] is equal to zero at $x>\bar{x}$. The source term I in Eq. (60) consists of two parts: the ionization by the fast electrons [Eq. (11)], which vanishes at $x>x_m$, and the ionization by the intermediate plasma electrons I_2, which switches on at $x>\bar{x}$ (Fig. 9). The FDS begins at the end of the fast-electron range R (12) and ends at $x=\bar{x}$.

In the main part of the NG and the FDS, the Boltzmann term in Eq. (61) dominates, and Eq. (60) reduces to the ambipolar diffusion equation (38). The electric-field profile is given by $E(x)=(T_e/e)d(\ln n)/dx$. This implies that the reversed field in the short discharge rises monotonically towards the anode. To our mind, this case corresponds to experiments [3]. The trapped-electron density is maximum at the field-reversal point. Since the main part of the source term in the kinetic equation (18) for the intermediate electrons is localized at $x<x_m$, their EDF (and density) is decreasing in the vicinity of x_m. Consequently, the field-reversal point in the low-pressure discharge is also shifted towards the anode with respect to x_m. The reason for the slight displacements of the field reversal towards the cathode, observed in Ref. [3], is not clear.

In the long discharge, the reversed field falls off as x increases, and the second field reversal occurs. In this case, the recombination in the FDS is significant. If the recombination on the chamber walls dominates, then $\tau=\Lambda^2/D_a$. The trapped-electron density decreases with the scale l_D, which is small compared to the intermediate-electron-density variation scale L_F given by Eq. (54) (see Fig. 9). In the vicinity of $x=\bar{x}$, where Eq. (38) is invalid, $n^{(i)}(x)$ can be approximated by a constant. Neglecting the density variation, we obtain from Eq. (60) that the potential profile here is parabolic,

$$\phi(x)=\frac{T_e U}{e}+\frac{(x-\bar{x})^2}{2\mu_i\tau_c} , \tag{62}$$

where τ_c is the value of $\tau=\Lambda^2/D_a$ corresponding to the FDS-PC boundary. The ambipolar diffusion coefficient in

τ_c corresponds to the temperature of the intermediate electrons. If their energy losses in the elastic collisions are negligible, this value is of the order of ε^*. The charged-particle lifetime τ_c at $x > \tilde{x}$ is considerably less ($\sim \varepsilon^*/T_e$ times) than τ in the main part of the FDS (which is determined by T_e).

In the region between $\bar{x}$ and $\tilde{x}$, the excitations are absent. The length of this part of the FDS with the direct field is

$$\bar{x} - \tilde{x} = L_F \left[\frac{\tau}{\tau_c} \ln \left[\frac{n_m}{n^{(i)}(\tilde{x})} \right] \right]^{-1/2} \ll L_F \ . \tag{63}$$

The field intensity at $x = \bar{x}$ is

$$\bar{E} = \frac{\bar{x} - \tilde{x}}{\mu_i \tau_c} = \frac{\Lambda}{\mu_i \tau_c} \left[\frac{T_e}{\varepsilon^*} \ln \left[\frac{n_m}{n^{(i)}(\tilde{x})} \right] \right]^{1/2} . \tag{64}$$

If this value is less than the field in the PC, E_c, then Eq. (60), with $n = n^{(i)}(x)$, instead of formula (61), describes the smooth field increase from $\bar{E}$ to E_c. In the opposite case, a field overshoot in the vicinity of $x = \bar{x}$ arises. Such a phenomenon was also predicted in Ref. [22].

The small deviation of the trapped-electron temperature from the uniform value is of the order of $(T_e - T_a) l_D / \lambda_\varepsilon$. It is due to the nonuniformity of the heating sources in Eq. (31). Since these sources are maximal at the NG-FDS boundary, the $T_e(x)$ profile in this case is decreasing towards the anode.

The precise form of the FDS-PC transition depends on the specific ionization and recombination processes. In the ionization model, when the charged-particle generation is correlated with the excitation rate (as in the case of stepwise ionization or when the ionization threshold is close to the excitation threshold), the simple mechanism of standing-striation formation is possible. If the FDS length is comparable with the energy-relaxation length λ_ε of the intermediate electrons, their energies in the vicinity of the field-reversal point $\tilde{x}$ are considerably less than ε^*. The ionization process begins at some point $\bar{\bar{x}} > \bar{x}$, ends at $x = x_0$ (Fig. 9), and is periodic in $e\phi$, with a period equal to ε^* [73]. Such spatially periodic plasma sources lead to the periodic-field profile in the PC that maintains the EDF periodicity in ε, owing to the mechanism of the EDF bunching [73]. As a result, the spatially periodic field profile and the EDF that is periodic in ε maintain each another, and a stable periodic solution arises [73]. A similar effect is possible even at $L_F \ll \lambda_\varepsilon$, since the intermediate electron sources, Eqs. (26) and (27), are nonuniform in the energy.

The distinction between the low- and high-pressure cases can be clearly seen if we compare the results of Refs. [6] and [74]. In Ref. [6], the numerical modeling has been performed for an Ar discharge at $p = 0.6$ Torr, $L = 2$ cm. The recombination and the ionization by the plasma electrons, I_2, were not included. Since the energy-relaxation length in the elastic collisions, $\lambda_\varepsilon > 10$ cm, far exceeded the gap length, this case corresponds to the short low-pressure discharge. In full accordance with the aforesaid, one field reversal was found. Its position was slightly shifted towards the anode with respect to the density maximum; the anode potential fall was negative.

In Ref. [74], the experiment and modeling have been performed for a discharge in H_2 at $p \sim 20$ Torr, $L = 2.0$ cm. The energy-relaxation length, accounting only for elastic losses, is, in this case, of the order of 0.03 cm (as was stated above, the genuine value of λ_ε can be considerably less). The diffusion length $l_D \sim \sqrt{D_a/\alpha_r n} = 0.1$ cm (α_r is the recombination rate constant) far exceeded λ_ε. This case corresponds to the long high-pressure discharge in our notation. In the modeling, the density decrease (and the field-magnitude increase) from the cathode in the FDS was found to occur on the scale of about 0.2 cm. The transition to the PC was also clearly seen. The anode fall was positive. All these facts were also observed in the experiment. A rough estimate for the ratio in Eq. (57) is of the order of unity. Accordingly, it was observed that the reversed-field region occupied only a small part of the FDS.

In numerous publications, the various forms of the slow-electron energy-transport equation were analyzed. Within the framework of our approach, such an equation is extraneous. In the high-pressure case, the local approximation is valid: all the characteristics of the slow electrons are defined by the local field. At low pressures, the energy transport results in the isothermicity of the trapped electrons. For the intermediate ones, a rigorous kinetic analysis is necessary.

Since the electron energy and density values in the NG-FDS-PC region vary by orders of magnitude, the presented view is very rough, and various intermediate situations are possible. The problem of energy transport in these cases needs additional investigation.

V. CONCLUSION

A simple self-consistent analytic model of the glow-discharge cathode region is suggested. It is demonstrated that the kinetic analysis of the electron motion is necessary for a correct description of the main characteristics of the discharge. Analytic solutions of the kinetic equation for the fast and slow electrons are derived. Simple expressions for the nonlocal ionization produced by the fast electrons are presented. It is shown that the field-reversal phenomenon is kinetic in origin, the criterion of its existence is derived, and the positions of the field-reversal points are estimated. The field overshoot on the FDS-PC boundary is predicted and the mechanism of the standing-striation formation is proposed.

[1] B. Barbiery, N. Beverini, and A. Sasso, Rev. Mod. Phys. **62**, 603 (1990).

[2] E. A. Den Hartog, D. A. Doughty, and J. E. Lawler, Phys. Rev. A **38**, 2471 (1988).

[3] R. A. Gottscho, A. Mitchell, G. R. Scheller, Y. Chan, and D. B. Graves, Phys. Rev. A **40**, 6407 (1989).

[4] E. A. Den Hartog, T. B. Brian, and J. W. Lawler, Phys. Rev. Lett. **62**, 1500 (1989); J. W. Lawler, E. A. Den Har-

tog, and W. N. G. Hitchon, Phys. Rev. A **43**, 4427 (1991).
[5] V. A. Schweigert and I. V. Schweigert, Fiz. Plazmy **14**, 347 (1988) [Sov. J. Plasma Phys. **14**, 204 (1988)]; Teplofiz. Vys. Temp. **27**, 23 (1989) [High. Temp. **27**, 21 (1989)].
[6] M. Surendra, D. B. Graves, and G. M. Gellum, Phys. Rev. A **41**, 1112 (1990).
[7] H. Debontride, J. Derouard, P. Edel, R. Romestain, N. Sadeghi, and J. P. Boeuf, Phys. Rev. A **40**, 5208 (1989); J. P. Boeuf, in *Physics and Applications of Pseudosparks,* Vol. 219 of *NATO Advanced Study Institute, Series B: Physics,* edited by M. A. Gundersen and G. Schaefer (Plenum, New York, 1990), p. 255.
[8] B. Shi, G. J. Fetzer, Z. Yu, J. D. Meyer, and G. J. Collins, IEEE J. Quantum Electron. **25**, 948 (1989).
[9] W. Weizel, R. Rompe, and M. Schon, Z. Phys. **112**, 339 (1939); **113**, 87 (1939); **113**, 730 (1939).
[10] K. G. Emeleus and W. L. Brown, Philos. Mag. **7**, 17 (1939).
[11] K. G. Emeleus, W. L. Brown, and Mc. N. Cowan, Philos. Mag. **17**, 146 (1934).
[12] D. H. Pringle and W. E. G. Farvis, Phys. Rev. **96**, 536 (1954).
[13] J. M. Anderson, J. Appl. Phys. **31**, 511 (1960).
[14] W. Stern, Beitr. Plasmaphys. **9**, 59 (1969).
[15] G. S. Solntsev, A. I. Orlov, and V. A. Dovzgenko, Radiotekh. Elektron. **9**, 1980 (1970); V. L. Granovskii, *Electric Current in Gas* (in Russian) (Nauka, Moscow, 1971).
[16] P. Gill and C. E. Webb, J. Phys. D **10**, 299 (1977).
[17] G. S. Evtushenko, A. G. Gridnev, and I. I. Murav'jev, Izv. Vyssh. Uchebn. Zaved. Fiz. (USSR) **9**, 80 (1975).
[18] P. Segur, M. Yousfi, J. P. Boeuf, E. Marode, A. J. Davies, and J. G. Evans, in *Electrical Breakdown and Discharges in Gases,* Vol. 89A of *NATO Advanced Study Institute, Series B: Physics,* edited by E. E. Kunhardt and L. H. Luessen (Plenum, New York, 1983), p. 331.
[19] R. G. Carman and A. Maitland, J. Phys. D **20**, 1021 (1987).
[20] J. V. DiCarlo and M. J. Kushner, J. Appl. Phys. **66**, 5763 (1989).
[21] T. J. Sommerer, W. N. G. Hitshon, and J. E. Lawler, Phys. Rev. A **39**, 6356 (1989).
[22] Y. P. Raizer and M. I. Schneider (unpublished); Teplofiz. Vys. Temp. **29**, 950 (1991).
[23] N. A. Tran, E. Marode, and P. C. Johnson, J. Phys. D **10**, 2317 (1977).
[24] J. P. Boeuf and E. Marode, J. Phys. D **15**, 2169 (1982).
[25] M. Ohuchi and T. Kubota, J. Phys. D **16**, 1705 (1983).
[26] G. Frank, Z. Phys. **218**, 460 (1969); **256**, 73 (1972).
[27] K. G. Emeleus, J. Phys. D **14**, 2179 (1981).
[28] P. F. Little and A. von Engel, Proc. R. Soc. London Ser. A **224**, 209 (1954).
[29] Y. P. Raizer, in Proceedings of the ICPIG XVII, Budapest, 1985, Invited Papers, p. 111; Teplofiz. Vys. Temp. **24**, 984 (1986) [High Temp. **24**, 744 (1986)].
[30] J. P. Boeuf, J. Appl. Phys. **63**, 1342 (1988).
[31] V. I. Kolobov and L. D. Tsendin, Zh. Tekh. Fiz. **59**, 22 (1989) [Sov. Phys. Tech. Phys. **34**, 1239 (1989)].
[32] A. V. Phelps, B. M. Jelenkovic, and L. C. Pitchford, Phys. Rev. A **36**, 5327 (1987).
[33] T. J. Sommerer, J. E. Lawler, and W. N. G. Hitchon, J. Appl. Phys. **64**, 1775 (1988).
[34] L. D. Landau and E. M. Lifshitz, *Quantum Mechanics—Non-Relativistic Theory* (Addison-Wesley, Reading, MA, 1965).
[35] N. P. Kalashnikov, V. S. Remizovich, and M. I. Rjazanov, *Collisions of Fast Charged Particles in Solids* (in Russian) (Atomizdat, Moscow, 1980).
[36] K. G. Muller, Z. Phys. **169**, 432 (1962).
[37] V. P. Konovalov and E. I. Son, in *Plasma Chemistry,* edited by B. M. Smirnov (Energoatomizdat, Moscow, 1987), Vol. 14, p. 194 [*Review of Plasma Chemistry* (Plenum, New York, 1991), Vol. 1, p. 219]; see also Radiat. Res. **64**, N1 (1975).
[38] E. E. Kunhardt and W. W. Byszewsky, Phys. Rev. A **21**, 2069 (1980).
[39] L. R. Peterson and A. E. S. Green, J. Phys. B **1**, 1131 (1968).
[40] W. T. Miles, R. Thompson, and A. E. S. Green, J. Appl. Phys. **43**, 678 (1972).
[41] A. E. S. Green, Radiat. Res. **64**, 6 (1975).
[42] A. E. S. Green and T. Sawada, J. Atmos. Terr. Phys. **34**, 1719 (1972).
[43] N. F. Mott and H. S. W. Massey, *The Theory of Atomic Collisions* (Clarendon, Oxford, 1965).
[44] L. Friedland, J. Phys. D **7**, 2246 (1974).
[45] Yu. M. Kagan, J. Phys. D **24**, 882 (1991).
[46] P. Bayle, J. Vacquie, and M. Bayle, Phys. Rev. A **34**, 360 (1986).
[47] D. B. Graves and K. F. Jensen, IEEE Trans. Plasma Sci. **14**, 78 (1986).
[48] M. Meyyappan and J. P. Kreskovsky, J. Appl. Phys. **68**, 1506 (1990).
[49] H. Neu, Z. Phys. **154**, 423 (1959); **155**, 77 (1959).
[50] S. Ya. Bronin and V. M. Kolobov, Fiz. Plazmy **9**, 1088 (1983) [Sov. J. Plasma Phys. **9**, 640 (1983)].
[51] A. K. Brever and J. W. Westhaver, J. Appl. Phys. **8**, 779 (1937).
[52] K. N. Ul'yanov and V. V. Chulkov, Teplofiz. Vys. Temp. **27**, 807 (1989).
[53] J. E. Lehmann, Proc. R. Soc. London **115**, 624 (1927).
[54] A. von Engel, *Ionized Gases* (Clarendon, Oxford, 1965).
[55] Y. P. Raizer, *Gas Discharge Physics* (Springer-Verlag, Berlin, 1991).
[56] C. N. Yang, Phys. Rev. **84**, 599 (1951).
[57] A. L. Hughes and W. Harris, Phys. Rev. **48**, 408 (1935).
[58] V. L. Ginzburg and A. V. Gurevich, Usp. Fiz. Nauk. **70**, 201 (1960) [Sov. Phys. Usp. **2**, 115 (1960)].
[59] I. B. Bernstein and T. Holstein, Phys. Rev. **94**, 1475 (1954).
[60] L. D. Tsendin, Zh. Eksp. Teor. Fiz. **66**, 1636 (1974) [Sov. Phys. JETP **39**, 805 (1974)].
[61] I. P. Shkarovsky, T. W. Johnston, and M. P. Bachinski, *The Particle Kinetics of Plasmas* (Addison-Wesley, Reading, MA, 1966).
[62] Y. B. Golubovskii, Yu. m. Kagan, and R. I. Lyagushchenko, Zh. Eksp. Teor. Fiz. **57**, 2222 (1969) [Sov. Phys. JETP **30**, 1204 (1970)].
[63] N. V. Bedenkov, N. B. Kolokolov, A. A. Kudryavtsev, and V. A. Romanenko, Zh. Tekh. Fiz. **58**, 2098 (1988) [Sov. Phys. Tech. Phys. **33**. 282 (1988)].
[64] N. B. Kolokolov and A. A. Kudryavtsev, in *Plasma Chemistry,* edited by B. M. Smirnov (Energoatomizdat, Moscow, 1989), Vol. 15, p. 127 [*Review of Plasma Chemistry* (Plenum, New York, 1992), Vol. 2, p. 1].
[65] Y. B. Golubovsky, S. H. al-Havat, and L. D. Tsendin, Zh. Tekh. Fiz. **57**, 1289 (1987) [Sov. Phys. Tech. Phys. **32**, 760 (1987)].
[66] R. I. Lyagushchenko, Zh. Eksp. Teor. Fiz. **63**, 1706 (1972) [Sov. Phys. JETP **36**, 901 (1973)].

[67] Yu. M. Kagan, C. Cohen, and P. J. Avivi, J. Appl. Phys. **63**, 60 (1988).
[68] Y. S. Akishev, F. I. Vysikailo, A. P. Napartovitch, and V. V. Ponomarenko, Teplofiz. Vys. Temp. **18**, 266 (1980) [High. Temp. **18**, 266 (1980)].
[69] A. P. Dmitriev, V. A. Rozhanskii, and L. D. Tsendin, Usp. Fiz. Nauk **146**, 237 (1985) [Sov. Phys. Usp. **28**, 467 (1985)]; V. A. Rozhanskii and L. D. Tsendin, *Collisional Transport in Partially-Ionized Plasma* (in Russian) (Energoatomizdat, Moscow, 1988).
[70] K.-U. Riemann, J. Phys. D **24**, 493 (1991).
[71] R. Warren, Phys. Rev. **98**, 1650 (1955).
[72] L. D. Tsendin, Zh. Tekh. Fiz. **56**, 278 (1986) [Sov. Phys. Tech. Phys. **31**, 169 (1986)].
[73] L. D. Tsendin, Fiz. Plazmy **8**, 400 (1982) [Sov. J. Plasma Phys. **8**, 228 (1982)].
[74] M. Surendra, D. B. Graves, and L. S. Plano, J. Appl. Phys. (to be published).